Supplemental Information

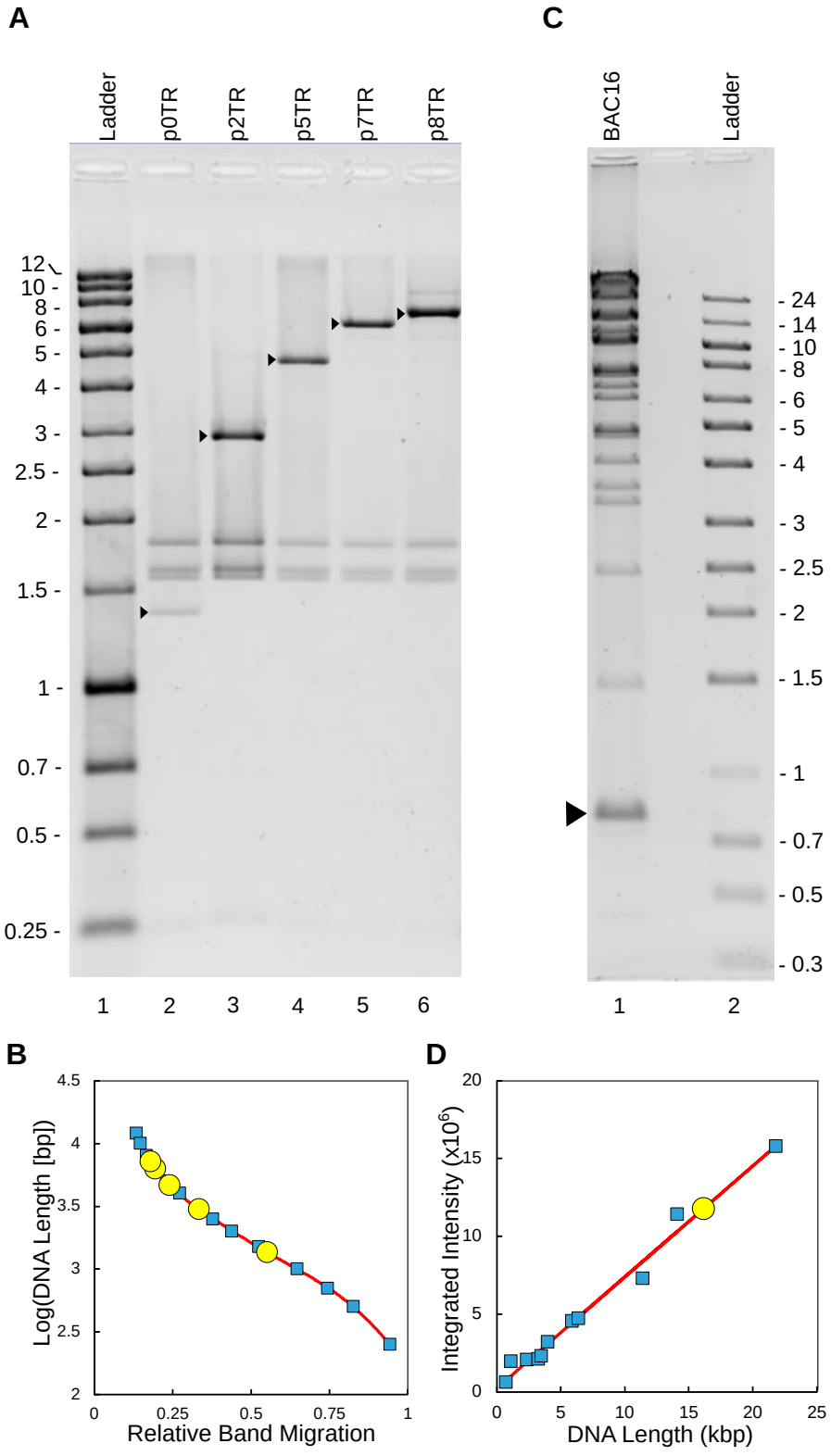

Figure S1, related to Figure 3. Number of TRs in each pNTR plasmid and BAC16

(A) Plasmids with variable (N) numbers of TRs (pNTR) were digested with PstI, which cuts on either side of the TR-containing insert. Length of the released fragment (arrowheads) allowed determination of TR number. Lane 1, ladder (kbp), lane 2, plasmid lacking TRs, lanes 3-6, plasmids with 2, 5, 7, and 8 TRs, respectively.

(B) Relative mobilities of DNA standards (blue squares) were used to construct a best-fit curve for the log of DNA length as a function of migration (red line). Lengths of PstI fragments from plasmids with variable numbers of TRs (yellow circles) were determined from the standard curve based on their migration.

(C) NotI + SpeI digest of BAC16 (lane 1), isolating the 801-bp TR fragments (arrowhead). Lane 2, ladder (kbp).

(D) The number of TRs within BAC16 was determined from the intensity of ethidium bromide staining. Fragments present once per BAC (blue squares) were used to determine a best-fit line (red) for band intensity as a function of DNA length ($R^2 = 0.98$). Intensity of the TR-containing fragment (yellow circle) was then mapped to this standard curve, yielding a calculation of 20 TRs per BAC16 genome.

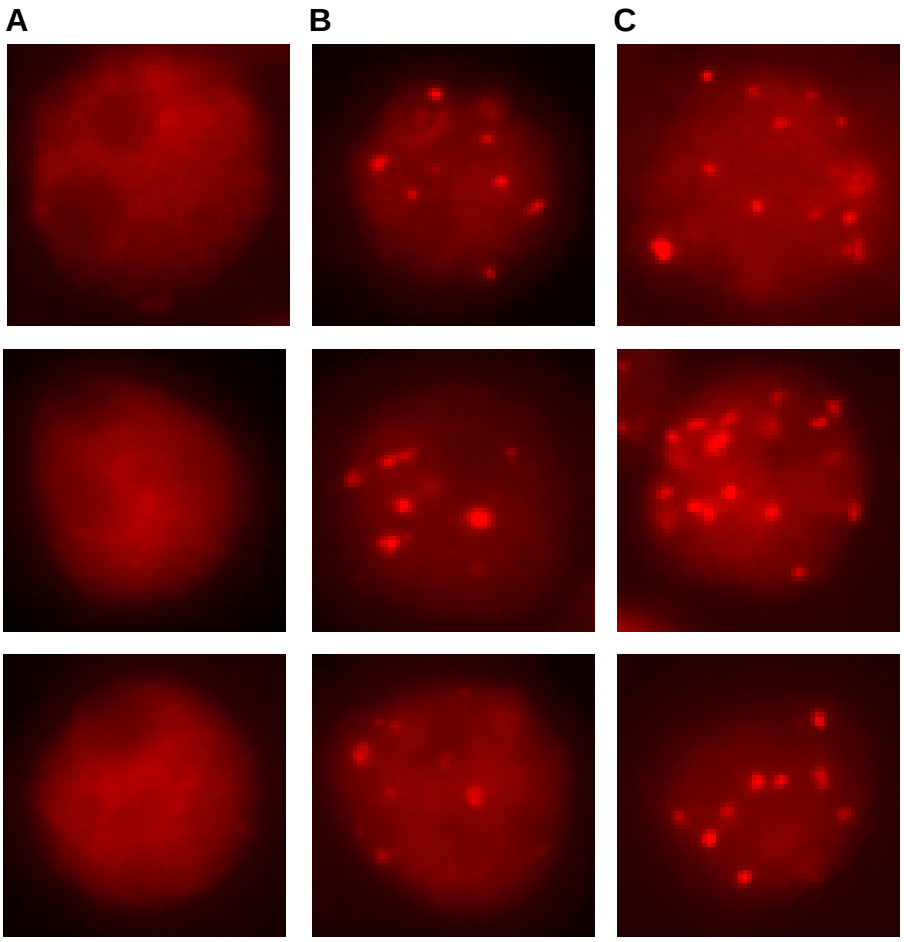

Figure S2, related to Figure 3. Punctate LANA tethers are visible only in the presence of TRs

(A-B) Epifluorescence images show three representative BJAB cells transfected with LANA-expressing plasmid plus either (A) p0TR plasmid, resulting in diffuse, non-punctate LANA staining, or (B) p8TR plasmid, resulting in punctate LANA staining.

(C) BJAB cells co-cultured with induced iSLK-BAC16 cells also resulted in punctate LANA staining.

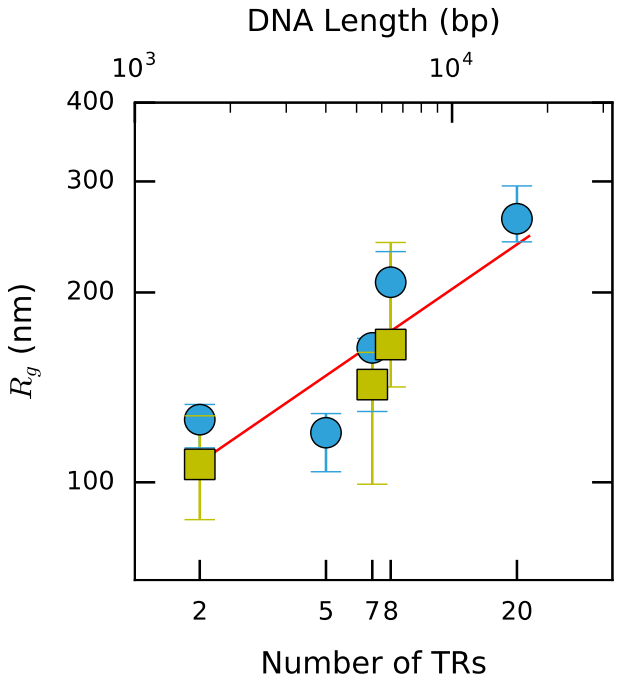

Figure S3, related to Figure 3. Scaling of R_g with increasing number of TRs in COS-7 cells supports the results seen in BJAB cells

A plot of R_g vs TR number for p2TR, p7TR, and p8TR in COS-7 (yellow squares), shown in comparison with the BJAB data (blue circles). The combined data yield a scaling exponent value of $c = 0.35 \pm 0.07$, $R^2 = 0.89$.

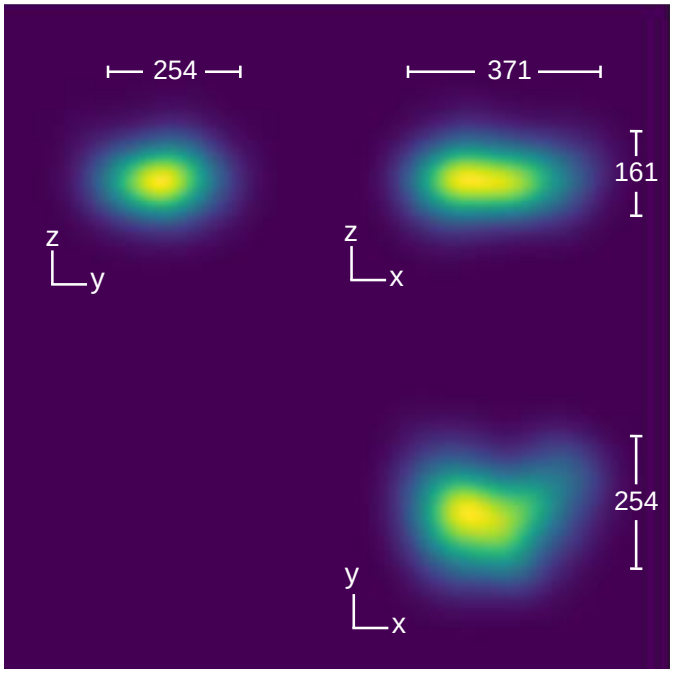

Figure S4, related to Figure 4. COS-7 p2TR data shows two clusters of emissions for each tether, similar to that seen in BJAB cells

Compilation of emission data from 16 p2TR tethers in COS-7 cells; emissions are rendered as in Figure 2. Median dimensions (nm) of the combined data are shown.

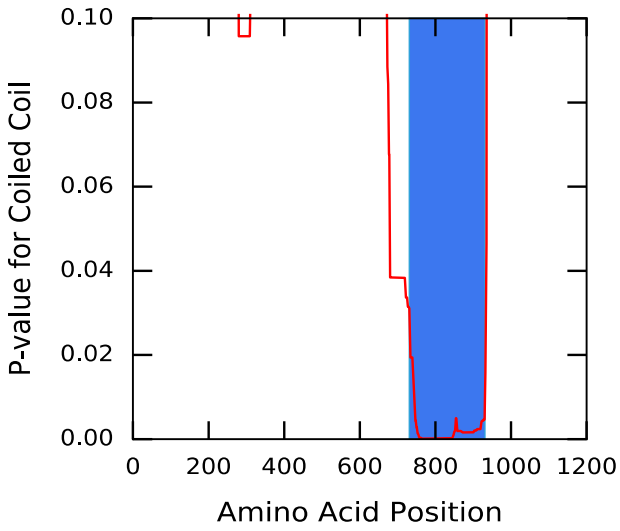

Figure S5, related to Figure 5. The predicted coiled-coil region in the LANA protein

A plot showing the location of the predicted coiled-coil structure (blue) in the LANA protein (Paircoil2; LANA sequence GenBank: U75698.1; P-value < 0.025).

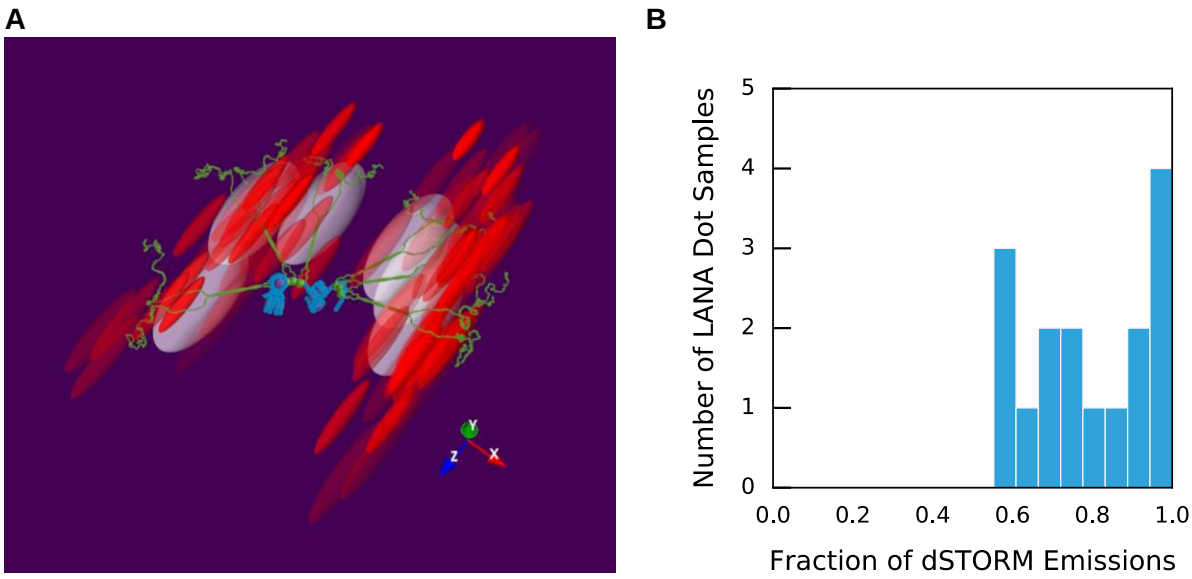

Figure S6, related to Figure 7. A model with full LBS and nucleosome occupancy on two sequential TRs supports dSTORM data from COS-7 cells

(A) Data from one p2TR example aligned with a model similar to that shown in Figure 7A. Red ellipsoids depict the probability volume of individual fluorophore emissions, scaled by their lateral and axial localization precision. White ellipsoids depict the model-predicted probability volumes scaled by data-derived localization precision.

(B) Histogram displaying the distribution of the fraction of observed emissions whose localization precision volumes intersect with the model-predicted volume. Median overlap fraction = 0.78, 95% CI [0.66, 0.94].

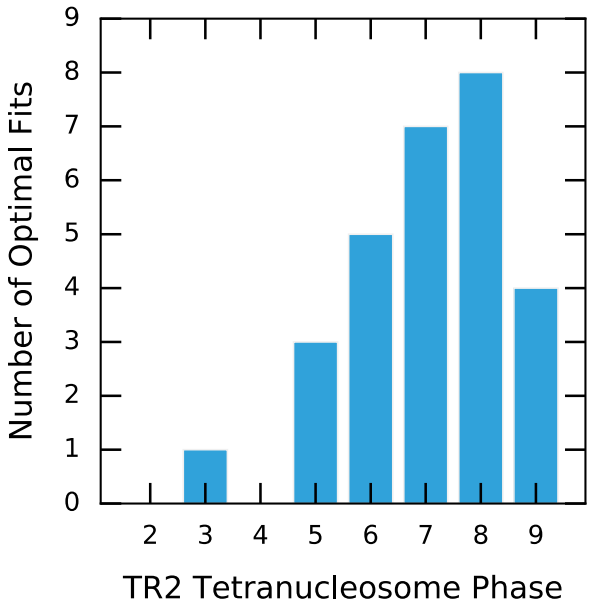

Figure S7, related to Figure 7. Multiple tetranucleosome translational positions are compatible with the p2TR dSTORM data in BJAB cells

Frequency with which different model tetranucleosome phases give rise to the optimal fit to the dSTORM p2TR data sets in BJAB cells. The compatibility of several different phase positions would facilitate the complex folding of higher order TR polymers.

Movie S1. Animation of the three-dimensional modeling of LANA binding to TR DNA and the resulting Ab-bound fluorophore emissions. Each of the many fluorophore emissions captured by dSTORM from a single 2TR example is presented as a red ellipsoid encompassing that emission's median three-dimensional localization precision. These data are superimposed on the model of 2TRs presented in Figure 7A and B. Emerging magenta spheres represent the 13 nm radius encompassing the potential localization of the bound anti-LANA mAb, as in Figure 7B. The video zooms in to more clearly show the architecture surrounding the TR DNA, LANA C-terminal LBS binding, and associated tetrasomes. Finally, white ellipsoids appear, denoting model-predicted fluorophore emissions at one standard deviation of the localization precision.